

# Population III.1 and III.2 Gamma-Ray Bursts: Constraints on the Event Rate for Future Radio and X-ray Surveys

R. S. de Souza<sup>1,2</sup>, N. Yoshida<sup>1</sup>, and K. Ioka<sup>3</sup>

<sup>1</sup>Institute for the Physics and Mathematics of the Universe, University of Tokyo, 5-1-5 Kashiwanoha, Kashiwa, Chiba 277-8583, Japan

<sup>2</sup>IAG, Universidade de São Paulo, Rua do Matão 1226, Cidade Universitária, CEP 05508-900, São Paulo, SP, Brazil

<sup>3</sup>KEK Theory Center and the Graduate University for Advanced Studies (Sokendai), Tsukuba 305-0801, Japan

Released Xxxxx XX

## ABSTRACT

**Aims.** We calculate the theoretical event rate of gamma-ray bursts (GRBs) from the collapse of massive first generation (Population III; Pop III) stars. The Pop III GRBs could be super-energetic with the isotropic energy up to  $E_{\text{iso}} \gtrsim 10^{55-57}$  ergs, providing a unique probe of the high redshift Universe.

**Methods.** We consider both the so-called Pop III.1 stars (which are primordial) and Pop III.2 stars (which are primordial but affected by radiation from other stars). We employ a semi-analytical approach taking into account inhomogeneous hydrogen reionization and chemical evolution of the inter-galactic medium.

**Results.** We show that Pop III.2 GRBs occur more than 10 times more frequently than Pop III.1 GRBs, and thus should be suitable targets for future GRB missions. Interestingly, our optimistic model predicts an event rate which is already constrained by the current radio transient searches. We expect  $\sim 10 - 1000$  radio afterglows above  $\sim 1\text{mJy}$  on the sky with  $\sim 1$  year variability and mostly without GRBs (orphan), which are detectable by ALMA, EVLA, LOFAR and SKA, while  $\sim 0.3-6$  events per year for the X-ray detections of the prompt emission by *Swift*, SVOM, JANUS and EXIST.

**Key words.** Population III; Gamma-ray burst; Radio lines; X-rays

## 1. Introduction

The first stars in the Universe are thought to have played a crucial role in the early cosmic evolution, by emitting the first light and producing the first heavy elements (Bromm et al. 2009). Theoretical studies based on the standard cosmological model predict that the first stars were formed when the age of the Universe was less than a few hundred million years, and that they were predominantly massive (Abel et al. 2002; Omukai & Palla 2003; Yoshida et al. 2006). Although there are a few observational ways to probe the early stellar populations, there has been yet no direct observations of the so-called Population III (Pop III) stars.

Recently, it was proposed that massive Pop III stars may produce collapsar gamma-ray bursts (GRBs), whose total isotropic energy could be  $E_{\text{iso}} \gtrsim 10^{55-57}$  ergs, i.e.,  $\gtrsim 2$  orders of magnitude larger than av-

erage (Komissarov & Barkov 2010; Toma et al. 2010; Mészáros & Rees 2010; Barkov 2010; Suwa & Ioka 2011). Even if the Pop III star has a supergiant hydrogen envelope, the GRB jet can break out the first star because of the long-lasting accretion of the envelope itself (Suwa & Ioka 2011; Nagakura et al. 2011). The observations of the spectral peak energy-peak luminosity relation also imply that GRBs actually occur at high redshift,  $z \gtrsim 10$  (Yonetoku et al. 2004).

Observations of such energetic GRBs at very high redshifts will provide a unique probe of the high redshift Universe (Lamb & Reichart 2000; Ciardi & Loeb 2000; Gou et al. 2004). Ioka & Mészáros (2005) study the radio afterglows of high-redshift GRBs and show that they can be observed out to  $z \sim 30$  by VLA<sup>1</sup>, LOFAR<sup>2</sup> and SKA<sup>3</sup> (see also Ioka (2003)). Inoue et al. (2007) calculate time-

<sup>1</sup> <http://www.vla.nrao.edu/>

<sup>2</sup> <http://www.lofar.org/index.htm>

<sup>3</sup> <http://www.skatelescope.org/>

dependent, broad-band afterglow spectra of high-redshift GRBs. They suggest that spectroscopic measurements of molecular and atomic absorption lines due to ambient protostellar gas may be possible to  $z \sim 30$  and beyond with ALMA<sup>4</sup>, EVLA<sup>5</sup>, and SKA. In the future, it will be also promising to observe the GRB afterglows located by gamma-ray satellites such as *Swift*<sup>6</sup>, SVOM<sup>7</sup>, JANUS<sup>8</sup> and EXIST<sup>9</sup>. Clearly, it is important to study the rate and the detectability of Pop III GRBs at very high redshifts.

There have been already a few observations of GRBs at high redshifts. GRB 090423, at a redshift of  $z = 8.26$  (Salvaterra et al. 2009; Tanvir et al. 2009), is the object with the second highest redshift observed to date after the discovered galaxy at  $z = 8.6$  (Lehnert et al. 2010), beyond the previous GRB 080913 at  $z = 6.7$  (Greiner et al. 2009), GRB 050904 at  $z = 6.3$  (Kawai et al. 2006; Totani et al. 2006) and the highest redshift quasar at  $z = 6.41$  (Willott et al. 2003). Chandra et al. (2010) reported the discovery of radio afterglow emission from GRB 090423, and Frail et al. (2006) for GRB 050904. Observations of afterglows make it possible to derive physical properties of the explosion and the circumburst medium. It is intriguing to search for these different signatures in the GRB afterglows at low and high redshifts.

The purpose of the present paper is to calculate the Pop III GRB rate detectable by the current and future GRB missions. We consider high-redshift GRBs of two populations following Bromm et al. (2009). Pop III.1 stars are the first generation stars that form from initial conditions determined cosmologically. Pop III.2 stars are zero-metallicity stars but formed from a primordial gas that was influenced by earlier generation of stars. Typically, Pop III.2 stars are formed in an initially ionized gas (Johnson & Bromm 2006; Yoshida et al. 2007). The Pop III.2 stars are thought to be less massive ( $\sim 40\text{--}60M_{\odot}$ ) than Pop III.1 stars ( $\sim 1000M_{\odot}$ ) but still massive enough for producing GRBs. We calculate the GRB rate for these two populations separately for the first time. The rest of the paper is organized as follows. In Sect. 2, we describe a semi-analytical model to calculate the formation rate of primordial GRBs. In Sect. 3, we show our model predictions and calculate the detectability of Pop III GRBs by future satellite missions and by radio observations. In Sect. 4, we discuss the results and give our concluding remarks. Throughout the paper we adopt the standard  $\Lambda$  Cold Dark Matter model with the best fit cosmological parameters from Jarosik et al. (2011) (WMAP-Yr7<sup>10</sup>),  $\Omega_m = 0.267$ ,  $\Omega_{\Lambda} = 0.734$ , and  $H_0 = 71\text{km s}^{-1}\text{Mpc}^{-1}$ .

## 2. Gamma-ray burst rate

We assume that the formation rate of GRBs is proportional to the star formation rate (Totani 1997). The number of observable GRBs per comoving volume per time is expressed as

$$\Psi_{\text{GRB}}^{\text{obs}}(z) = \frac{\Omega_{\text{obs}}}{4\pi} \eta_{\text{GRB}} \eta_{\text{beam}} \Psi_*(z) \int_{L_{\text{lim}}(z)}^{\infty} p(L) dL, \quad (1)$$

where  $\eta_{\text{GRB}}$  is the GRB formation efficiency (see section 2.6),  $\eta_{\text{beam}}$  is the beaming factor of the burst,  $\Omega_{\text{obs}}$  is the field of view of the experiment,  $\Psi_*$  is the cosmic star formation rate (SFR) density and  $p(L)$  is the GRB luminosity function in X-rays to gamma-rays. The intrinsic GRB rate is given by

$$\Psi_{\text{GRB}}(z) = \eta_{\text{GRB}} \Psi_*(z). \quad (2)$$

The quantity  $L_{\text{lim}}(z)$  is the minimum luminosity threshold to be detected, which is specified for a given experiment. The non-isotropic nature of GRBs gives  $\eta_{\text{beam}} \sim 0.01 - 0.02$  (Guetta et al. 2005). Using a radio transients survey Gal-Yam et al. (2006) place an upper limit of  $\eta_{\text{beam}} \lesssim 0.016$ . We set  $\eta_{\text{beam}} = 0.015$  as a fiducial value. The adopted values of  $\Omega_{\text{obs}}$  are 1.4, 2, 4 and 5 for *Swift*, SVOM, JANUS and EXIST respectively (Salvaterra et al. 2008).

### 2.1. The number of collapsed objects

We first calculate the star formation rate (SFR) at early epochs. Assuming that stars are formed in collapsed dark matter haloes, we follow a popular prescription in which the number of collapsed objects is calculated by the halo mass function (Hernquist & Springel 2003; Greif & Bromm 2006; Trenti & Stiavelli 2009). We adopt the Sheth-Tormen mass function,  $f_{\text{ST}}$ , (Sheth & Tormen 1999) to estimate the number of dark matter haloes,  $n_{\text{ST}}(M, z)$ , with mass less than  $M$  per comoving volume at a given redshift:

$$f_{\text{ST}} = A \sqrt{\frac{2a_1}{\pi}} \left[ 1 + \left( \frac{\sigma^2}{a_1 \delta_c^2} \right)^p \right] \frac{\delta_c}{\sigma} \exp \left[ -\frac{a_1 \delta_c^2}{2\sigma^2} \right], \quad (3)$$

where  $A = 0.3222$ ,  $a_1 = 0.707$ ,  $p = 0.3$  and  $\delta_c = 1.686$ . The mass function  $f_{\text{ST}}$  can be related to the  $n_{\text{ST}}(M, z)$  as

$$f_{\text{ST}} = \frac{M}{\rho_m} \frac{dn_{\text{ST}}(M, z)}{d \ln \sigma^{-1}}, \quad (4)$$

where  $\rho_m$  is the total mass density of the background Universe. The variance of the linear density field  $\sigma(M, z)$  is given by

$$\sigma^2(M, z) = \frac{b^2(z)}{2\pi^2} \int_0^{\infty} k^2 P(k) W^2(k, M) dk, \quad (5)$$

where  $b(z)$  is the growth factor of linear perturbations normalized to  $b = 1$  at the present epoch, and  $W(k, M)$  is the Fourier-space top hat filter. To calculate the power spectrum  $P(k)$ , we use the CAMB code<sup>11</sup> for our assumed  $\Lambda$ CDM cosmology.

<sup>11</sup> <http://camb.info/>

<sup>4</sup> [www.alma.nrao.edu/](http://www.alma.nrao.edu/)

<sup>5</sup> <http://www.aoc.nrao.edu/evla/>

<sup>6</sup> <http://swift.gsfc.nasa.gov/docs/swift/swiftsc.html>

<sup>7</sup> <http://www.svom.fr/svom.html>

<sup>8</sup> <http://sms.msfc.nasa.gov/xenia/pdf/CCE2010/Burrows.pdf>

<sup>9</sup> <http://exist.gsfc.nasa.gov/design/>

<sup>10</sup> <http://lambda.gsfc.nasa.gov/product/map/current/>

## 2.2. H<sub>2</sub> Photodissociation

The star formation efficiency in the early Universe largely depends on the ability of a primordial gas to cool and condense. Hydrogen molecules (H<sub>2</sub>) are the primary coolant in a gas in small mass “minihaloes”. H<sub>2</sub> are also fragile to soft ultra-violet radiation, and thus a ultra-violet background in the Lyman-Werner (LW) bands can easily suppress the star formation inside minihaloes. We model the dissociation effect by setting the minimum mass for haloes that are able to host Pop III stars (Yoshida et al. 2003).

For the minimum halo mass capable of cooling by molecular hydrogen in the presence of a Lyman-Werner (LW) background, we adopt a fitting formula given by Machacek et al. (2001); Wise & Abel (2005), which is also in agreement with results from O’Shea & Norman (2008):

$$M_{\text{H}_2} = \exp\left(\frac{f_{\text{cd}}}{0.06}\right)(1.25 \times 10^5 + 8.7 \times 10^5 F_{\text{LW},-21}^{0.47}), \quad (6)$$

where  $F_{\text{LW},-21} = 4\pi J_{\text{LW}}$  is the flux in the LW band in units of  $10^{-21} \text{erg}^{-1} \text{s}^{-1} \text{cm}^{-2} \text{Hz}^{-1}$ ,  $f_{\text{cd}}$  is the fraction of gas that is cold and dense. We set  $f_{\text{cd}} = 0.02$  as a conservative estimate. We compute the LW flux consistently with the comoving density in stars  $\rho_*(z)$  via a conversion efficiency  $\eta_{\text{LW}}$  (Greif & Bromm 2006):

$$J_{\text{LW}} = \frac{hc}{4\pi m_{\text{H}}} \eta_{\text{LW}} \rho_*(z) (1+z)^3. \quad (7)$$

Here,  $\eta_{\text{LW}}$  is the number of photons emitted in the LW bands per stellar baryon and  $m_{\text{H}}$  is the mass of hydrogen. The value of  $\eta_{\text{LW}}$  depends on the characteristic mass of the formed primordial stars, but the variation is not very large for stars with masses greater than ten solar-masses (Schaerer 2002). We set  $\eta_{\text{LW}} = 10^4$  for both Pop III.1 and Pop III.2 for simplicity.

Next we calculate the stellar mass density as

$$\rho_*(z) = \int \Psi_*(z') \left| \frac{dt}{dz'} \right| dz'. \quad (8)$$

For a given  $z$ , the integral is performed over the maximum distance that a LW photon can travel before it is redshifted out of the LW bands. The mean free path of LW photons at  $z = 30$  is  $\sim 10$  Mpc (physical). Photons travel over the mean free path in  $\sim 10^7$  yr (Mackey et al. 2003). Haloes with virial temperature less than  $10^4$  Kelvin cool almost exclusively by H<sub>2</sub> line cooling, and produce mostly massive stars. We adopt the mass of such haloes,  $M(T_{\text{vir}} = 10^4 \text{K}, z)$ , as an upper limit of haloes that produce Pop III.1 stars. In larger haloes, the gas is ionized at virialization, and thus the formed stars have, according to our definition, similar properties to Pop III.2 stars. We assume that  $M(T_{\text{vir}} = 10^4 \text{K}, z)$  is the minimum halo mass for Pop III.2 star formation.

The collapsed fraction of mass,  $F_{\text{col}}(z)$ , available for Pop III star formation is given by

$$F_{\text{col}}^{\text{III.1}}(z) = \frac{1}{\rho_{\text{m}}} \int_{M_{\text{H}_2}}^{M_{T_{\text{vir}}=10^4\text{K}}} dM M n_{\text{ST}}(M, z), \quad (9)$$

for Pop III.1 stars, and

$$F_{\text{col}}^{\text{III.2}}(z) = \frac{1}{\rho_{\text{m}}} \int_{M_{T_{\text{vir}}=10^4\text{K}}}^{\infty} dM M n_{\text{ST}}(M, z), \quad (10)$$

for Pop III.2. Using the above criteria, the SFR of Pop III stars can be written as

$$\Psi_*^{\text{III.1}}(z) = (1 - Q_{\text{HII}}(z))(1 - \zeta(z, v_{\text{wind}})) \rho_{\text{m}} f_b f_* \frac{dF_{\text{col}}^{\text{III.1}}}{dt}, \quad (11)$$

for Pop III.1 stars, and

$$\Psi_*^{\text{III.2}}(z) = Q_{\text{HII}}(z)(1 - \zeta(z, v_{\text{wind}})) \rho_{\text{m}} f_b f_* \frac{dF_{\text{col}}^{\text{III.2}}}{dt}, \quad (12)$$

for Pop III.2. Here,  $\zeta(z, v_{\text{wind}})$  represents the global filling fraction of metals via galactic winds (see section 2.4),  $Q_{\text{HII}}(z)$  is volume filling fraction of ionized regions (see section 2.3) and  $f_b$  is the baryonic mass fraction. For the star formation efficiency, we use the value  $f_* = 0.001$  as a conservative choice (Greif & Bromm 2006) and  $f_* = 0.1$  (Bromm & Loeb 2006) as an upper limit. Note that the latter choice is not strictly consistent with the assumption made in Eq. (6). We explore a model with  $f_* = 0.1$  simply to show a very optimistic case.

## 2.3. Reionization

Inside growing HII regions, the gas is highly ionized and the temperature is  $\sim 10^4$  K, and thus the formation of Pop III.1 stars is terminated according to our definition. The formation rate of Pop III.1 is reduced by a factor given by the volume filling fraction of ionized regions,  $Q_{\text{HII}}(z)$ . We follow Wyithe & Loeb (2003) to calculate the evolution of  $Q_{\text{HII}}(z)$  as

$$\frac{dQ_{\text{HII}}}{dz} = \frac{N_{\text{ion}}}{0.76} \frac{dF_{\text{col}}}{dt} - \alpha_{\text{B}} \frac{C}{a^3} n_{\text{H}}^0 Q_{\text{HII}}, \quad (13)$$

whose solution is

$$Q_{\text{HII}}(z) = \int_z^{\infty} dz' \frac{dt}{dz'} \frac{N_{\text{ion}}}{0.76} \frac{dF_{\text{col}}}{dt} e^{F(z', z)}, \quad (14)$$

where

$$F(z', z) = -\frac{2}{3} \frac{\alpha_{\text{B}} n_{\text{H}}^0}{\sqrt{\Omega_{\text{m}}} H_0} C [f(z') - f(z)], \quad (15)$$

and

$$f(z) = \sqrt{(1+z)^3 + \frac{1 - \Omega_{\text{m}}}{\Omega_{\text{m}}}}. \quad (16)$$

Here we have assumed the primordial fraction of hydrogen of 0.76. In the above equations,  $N_{\text{ion}} \equiv N_{\gamma} f_* f_{\text{esc}}$  is an efficiency parameter that gives the number of ionizing photons per baryon, where  $f_{\text{esc}}$  is the fraction of ionizing photons able to escape the host galaxy,  $N_{\gamma}$  is the time averaged number of ionizing photons emitted per unit stellar mass formed. The quantity  $n_{\text{H}}^0 = 1.95 \times 10^{-7} \text{cm}^{-3}$  is the present-day comoving number density of hydrogen,  $\alpha_{\text{B}} = 2.6 \times 10^{-13} \text{cm}^3 \text{s}^{-1}$  is the hydrogen recombination

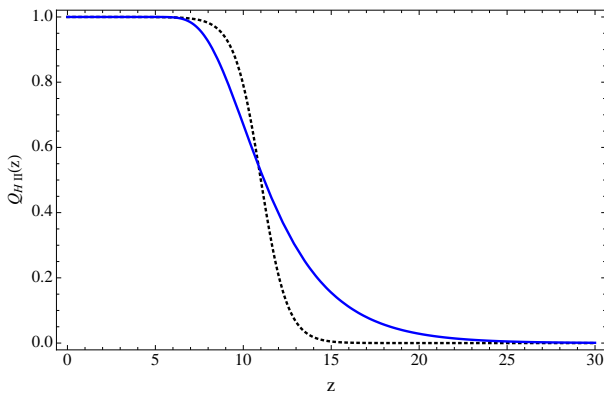


**Fig. 1.** Reionization history calculated using our model. The blue line is our model prediction, whereas the dotted black line is the best fit of CAMB code.

rate, and  $C = \langle n_{\text{H}}^2 \rangle / \bar{n}_{\text{H}}^2$  is the clumping factor. We use the average value  $C = 4$  (see Pawlik et al. (2009) for detailed discussion about redshift dependence of  $C$ ). We set the values  $f_{\text{esc}} = 0.7$ ,  $f_* = 0.01$  and  $N_\gamma = 9 \times 10^4$  as fiducial values (Greif & Bromm 2006).

In Fig. 1 we show the reionization history calculated using our model in comparison with a fitting function that is the default parametrization of reionization in CAMB (Lewis et al. 2000).

#### 2.4. Metal Enrichment

We need to consider metal-enrichment in the inter-galactic medium (IGM) in order to determine when the formation of primordial stars is terminated (locally) and when the star formation switches from the Pop III mode to a more conventional mode.

It is thought that Pop III stars do not generate strong stellar winds, and thus the main contribution to the metal pollution comes from their supernova explosions. Madau et al. (2001) argue that pre-galactic outflows from the same primordial haloes that reionize the IGM could also pollute it with a substantial amount of heavy elements. To incorporate the effect of metal-enrichment by galactic winds, we adopt a similar prescription of Johnson (2010); Furlanetto & Loeb (2005).

We assume that star-forming haloes (“galaxies”) launch a wind of metal-enriched gas at  $z_* \sim 20$ . The metal-enriched wind propagates outward from a central galaxy with a velocity  $v_{\text{wind}}$ , traveling over a comoving distance  $R_{\text{wind}}$  given by

$$R_{\text{wind}} = \int_{z_*}^z v_{\text{wind}}(1+z') \frac{dt}{dz'} dz'. \quad (17)$$

Then we can express  $f_{\text{chem}}$ , the ratio of gas mass enriched by the wind to the total gas mass in each halo, as

$$f_{\text{chem}}(M, z, v_{\text{wind}}) = \frac{4\pi R_{\text{wind}}^3}{3 V_{\text{H}}}, \quad (18)$$

where  $V_{\text{H}} \propto R_{\text{H}}^3$  is the volume of each halo. The halo radius  $R_{\text{H}}$  can be approximated by

$$R_{\text{H}}(M) = \left( \frac{3M}{4\pi \times 180\rho_{\text{m}}} \right)^{1/3}. \quad (19)$$

The fraction of cosmic volume enriched by the winds can then be written as

$$\zeta(z, v_{\text{wind}}) = \frac{1}{\rho_{\text{m}}} \int dM f_{\text{b}} f_* f_{\text{chem}}(M, z, v_{\text{wind}}) M n_{\text{ST}}(M, z). \quad (20)$$

Although this may appear a significant over-simplification, the model, with  $v_{\text{wind}}$  as a single parameter, indeed provides a good insight into the impact of the metal-enrichment.

We adopt three different values of  $v_{\text{wind}}$  and examine the effect of metal-enrichment quantitatively. We assume that Pop III stars are not formed in a metal-enriched region, regardless of the actual metallicity. We effectively assume that the so-called critical metallicity is very low (Bromm & Loeb 2003; Omukai et al. 2005; Frebel et al. 2007; Belczynski et al. 2010).

Fig. 2 and 3 show the star formation rate (SFR) history for both Pop III.1 and Pop III.2 considering three different values of the galactic wind,  $v_{\text{wind}} = 50, 75, 100$  km/s. Fig. 2 shows that the metal enrichment has a small influence over Pop III.1. This is because Pop III.1 formation is terminated early due reionization. We compare our model results with the SFRs estimated by other authors in the literature (Bromm & Loeb (2006); Tornatore et al. (2007); Trenti & Stiavelli (2009), see also Naoz & Bromberg (2007)). It is important to note that Pop III formation can continue to low redshifts ( $z < 10$ ) depending on the level of metal enrichment. Tornatore et al. (2007) used cosmological simulations to show that, because of limited efficiency of heavy element transport by outflows, Pop III star formation continues to form down to  $z = 2.5$  (which intriguingly matches with our model with  $v_{\text{wind}} = 50$  km/s in Fig. 3). The SFR of Tornatore et al. (2007) has a peak value of  $10^{-5} M_{\odot} \text{yr}^{-1} \text{Mpc}^{-3}$  at  $z \approx 6$  (the thin brown dot-dashed line in Figs. 2 and 3).

We also show the result of our model with  $f_* = 0.1$  and  $v_{\text{wind}} = 50$  km/s for both Pop III.1 and Pop III.2. This model provides an “optimistic” estimate for the detectable GRB rate for the future missions (see Sect. 3).

#### 2.5. Luminosity Function

The number of GRBs detectable by any given instrument depends on the instrument-specific flux sensitivity threshold and also on the intrinsic isotropic luminosity function of GRBs. For the latter, we adopt a power-law distribution function of Wanderman & Piran (2010)

$$p(L) = \begin{cases} \left( \frac{L}{L_*} \right)^{-0.2} & L < L_*, \\ \left( \frac{L}{L_*} \right)^{-1.4} & L > L_*. \end{cases}, \quad (21)$$

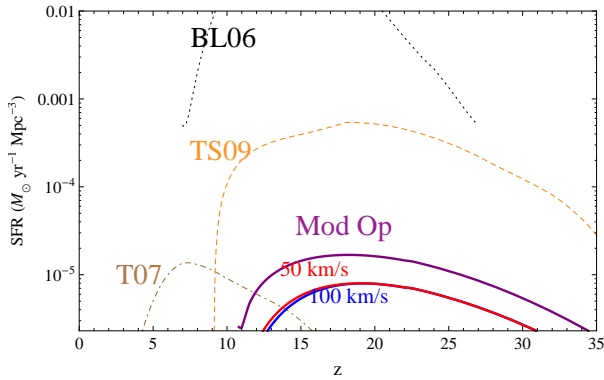


**Fig. 2.** Pop III.1 star formation rate for weak and strong chemical feedback models and a moderate star formation efficiency with  $f_* = 0.05$ . The results are shown for  $v_{\text{wind}} = 50$  km/s (red line) and 100 km/s (blue line). We also show the theoretical SFRs in the literature, from Bromm & Loeb 2006 (Pop III.1+III.2), dotted black line, Trenti & Stiavelli 2009 (Pop III.2), dashed orange line, and Tornatore et al. 2007 (Pop III.1+III.2), dot-dashed brown line. The purple line is our optimistic model where we assume a very high star formation efficiency,  $f_* \sim 0.1$ , and low chemical enrichment,  $v_{\text{wind}} = 50$  km/s.

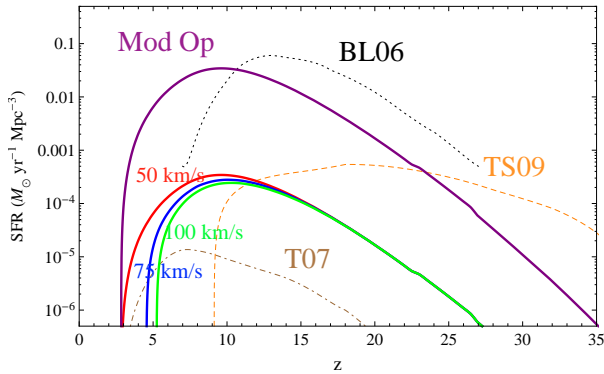


**Fig. 3.** Pop III.2 star formation rate for three different chemical feedback models;  $v_{\text{wind}} = 50$  km/s (red line)  $v_{\text{wind}} = 75$  km/s (blue line) and  $v_{\text{wind}} = 100$  km/s (green line). We also show the theoretical SFRs in the literature, from Bromm & Loeb 2006 (Pop III.1+III.2), dotted black line, Trenti & Stiavelli 2009 (Pop III.2), dashed orange line, and Tornatore et al. 2007 (Pop III.1+III.2), dot-dashed brown line. The purple line is our optimistic model where we assume a very high star formation efficiency,  $f_* \sim 0.1$ , and low chemical enrichment,  $v_{\text{wind}} = 50$  km/s.

where  $L_*$  is the characteristic isotropic luminosity. We set  $L_* \sim 10^{53}$  ergs/s for Pop III.1 whereas  $L_* \sim 10^{52}$  ergs/s Pop III.2 stars similar to ordinary GRBs (Li 2008; Wanderman & Piran 2010). Note that the Pop III.1 GRBs are assumed to be energetic with isotropic kinetic energy  $E_{\text{iso}} \sim 10^{56-57}$  erg but long-lived  $T_{90} \sim 1000$  s. So that the luminosity would be moderate  $L_* \sim \epsilon_\gamma \times 10^{56-57}/1000 \sim$

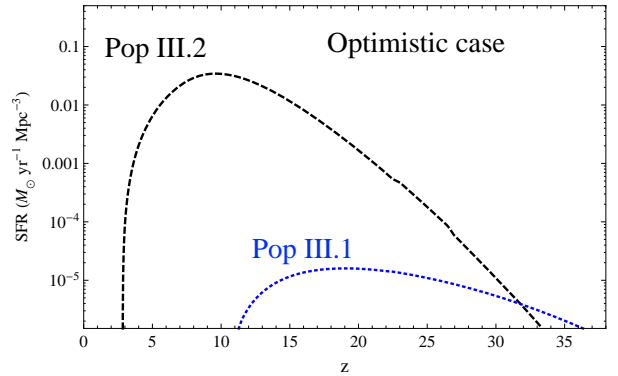


**Fig. 4.** We compare the star formation rates for Pop III.1 (blue dotted line) and for Pop III.2 (dashed black line), for our optimistic model with a high star formation efficiency  $f_* = 0.1$  and slow chemical enrichment  $v_{\text{wind}} = 50$  km/s.

$10^{52-53}$  ergs/s if  $\epsilon_\gamma \sim 0.1$  is the conversion efficiency from the jet kinetic energy to gamma rays (Suwa & Ioka 2011).

Using the above relation we can predict the observable GRB rate for *Swift*, SVOM, JANUS and EXIST missions. For *Swift*, we set a bolometric energy flux limit  $F_{\text{lim}} = 1.2 \times 10^{-8}$  erg cm $^{-2}$  s $^{-1}$  (Li 2008). We adopt a similar limit for SVOM (Paul et al. 2011). For JANUS,  $F_{\text{lim}} \sim 10^{-8}$  erg cm $^{-2}$  s $^{-1}$  (Falcone et al. 2009). The luminosity threshold is then

$$L_{\text{lim}} = 4\pi d_L^2 F_{\text{lim}}. \quad (22)$$

Here  $d_L$  is the luminosity distance for the adopted  $\Lambda$ CDM cosmology. EXIST is expected to be  $\sim 7 - 10$  times more sensitive than *Swift* (Grindlay 2010). We set the EXIST sensitivity threshold is 10 times lower than *Swift* as an approximate estimate.

## 2.6. Initial Mass Function and GRB Formation Efficiency

The stellar initial mass function (IMF) is critically important to determine the Pop III GRB rate. We define the GRB formation efficiency factor per stellar mass as

$$\eta_{\text{GRB}} = f_{\text{GRB}} \frac{\int_{M_{\text{GRB}}}^{M_{\text{up}}} \phi(m) dm}{\int_{M_{\text{low}}}^{M_{\text{up}}} m \phi(m) dm}, \quad (23)$$

where  $\phi(m)$  is the stellar IMF, and  $f_{\text{GRB}} = 0.001$  is the GRB fraction, since we expect 1 GRB every 1000 supernovae (Langer & Norman 2006). We assume that Pop III GRBs have a similar fraction.

We consider the following two forms of IMF. One is a power law with the standard Salpeter slope

$$\phi(m) \propto m^{-2.35}, \quad (24)$$

and the other is a Gaussian IMF (Scannapieco et al. 2003; Nakamura & Umemura 2001):

$$\phi(m) m^{-1} dm = \frac{1}{\sqrt{2\pi}\sigma_c(M)} e^{-(m-\bar{M})^2/2\sigma_c(M)^2} dm. \quad (25)$$

For the latter, we assume  $\bar{M} = 550M_\odot$  for Pop III.1 and  $\bar{M} = 55M_\odot$  for Pop III.2, with dispersion  $\sigma_c = (\bar{M} - M_{\text{low}})/3$ .  $M_{\text{low}}$  is the minimum mass for a given stellar type,  $100M_\odot$  for Pop III.1 and  $10M_\odot$  for Pop III.2, whereas  $M_{\text{up}}$  is the maximum mass for a given stellar type,  $1000M_\odot$  for Pop III.1 and  $\sim 100M_\odot$  for Pop III.2.  $M_{\text{GRB}}$  is the minimum mass that is able to trigger GRBs, which we set to be  $25M_\odot$  (Bromm & Loeb 2006). Note that not all Pop III.1 stars will leave a black hole behind at their deaths. In the narrow mass range of  $\sim 140 - 260M_\odot$  Pop III stars are predicted to undergo a pair-instability supernova (PISN) explosion (Heger & Woosley 2002). This range of mass is excluded from the calculation of Eq. (23).

The efficiency factor for the power-law (Salpeter) IMF is  $\eta_{\text{GRB}}/f_{\text{GRB}} \sim 1/926M_\odot^{-1}$  and  $1/87M_\odot^{-1}$  for Pop III.1 and Pop III.2 respectively. Using the gaussian IMF,  $\eta_{\text{GRB}}/f_{\text{GRB}} \sim 1/538M_\odot^{-1}$  and  $1/53M_\odot^{-1}$  for Pop III.1 and Pop III.2. respectively. Thus, the GRB formation efficiency for Pop III.2 can be about an order of magnitude larger than Pop III.1 because of the lower characteristic mass of Pop III.2 stars.

### 3. Redshift Distribution of GRBs

Over a particular time interval,  $\Delta t_{\text{obs}}$ , in the observer rest frame, the number of observed GRBs originating between redshifts  $z$  and  $z + dz$  is

$$\frac{dN_{\text{GRB}}^{\text{obs}}}{dz} = \Psi_{\text{GRB}}^{\text{obs}}(z) \frac{\Delta t_{\text{obs}} dV}{1+z dz}, \quad (26)$$

where  $dV/dz$  is the comoving volume element per unit redshift, given by

$$\frac{dV}{dz} = \frac{4\pi c d_L^2}{(1+z)} \left| \frac{dt}{dz} \right|. \quad (27)$$

Fig. 5 shows the intrinsic GRB rate

$$\frac{dN_{\text{GRB}}}{dz} = \Psi_{\text{GRB}}(z) \frac{\Delta t_{\text{obs}} dV}{1+z dz}. \quad (28)$$

In this plot, we have not considered observational effects such as beaming and instrument sensitivity. Namely, we set  $\Omega_{\text{obs}} = 4\pi$ ,  $\eta_{\text{beam}} = 1$  and  $L_{\text{lim}}(z) = 0$  in Eq. (1). We show the GRB rate for our choice of two different IMFs. Interestingly, Fig. 5 shows that the results depend only weakly on the choice of IMF.

Fig. 6 shows the most optimistic case, assuming a high star formation efficiency  $f_* \sim 0.1$ , an inefficient chemical enrichment,  $v_{\text{wind}} = 50$  km/s, and a gaussian IMF for both Pop III.1 and Pop III.2 stars. We note that constraints on these quantities will be useful to place upper limits on the GRB observed rate.

#### 3.1. Radio Afterglows

Follow-up observations of high redshift GRBs can be done by observing their afterglows especially in radio band (Ioka & Mészáros 2005; Inoue et al. 2007). We calculate

the radio afterglow light-curves for Pop III GRBs following the standard prescription from Sari et al. (1998, 1999); Mészáros (2006). The afterglow light-curve at the time  $t_d$  is given by the shock radius  $r_d$  and the Lorentz factor  $\gamma_d$ . These two quantities are related by  $E_{\text{iso}} \sim 4\pi r_d^3 \gamma_d^2 n m_p c^2$  and  $r_d \sim c \gamma_d^2 t_d$ , where  $n$  is the medium density and  $m_p$  is the proton mass. The true energy is given by  $E_{\text{true}} = \theta^2 E_{\text{iso}}/2$ , where  $\theta$  is the half opening angle of the shock. The spectrum consists of power-law segments linked by critical break frequencies. These are  $\nu_a$  (the self absorption frequency),  $\nu_m$  (the peak of injection frequency) and  $\nu_c$  (the cooling frequency), given by

$$\begin{aligned} \nu_m &\propto (1+z)^{1/2} g(p)^2 \epsilon_e^2 \epsilon_B^{1/2} E_{\text{iso}}^{1/2} t_d^{-3/2}, \\ \nu_c &\propto (1+z)^{-1/2} \epsilon_B^{-3/2} n^{-1} E_{\text{iso}}^{-1/2} t_d^{-1/2}, \\ \nu_a &\propto (1+z)^{-1} \epsilon_e^{-1} \epsilon_B^{1/5} n^{3/5} E_{\text{iso}}^{1/5}, \\ F_{\nu, \text{max}} &\propto (1+z) \epsilon_B^{1/2} n^{1/2} E_{\text{iso}} d_L^{-2}, \end{aligned} \quad (29)$$

where  $g(p) = (p-2)/(p-1)$ , is a function of energy spectrum index of electrons ( $N(\gamma_e) d\gamma_e \propto \gamma_e^{-p} d\gamma_e$ , where  $\gamma_e$  is the electron Lorentz factor),  $\epsilon_e$  and  $\epsilon_B$  are the efficiency factors (Mészáros 2006). There are two types of spectra. If  $\nu_m < \nu_c$ , we call it the *slow cooling case*. The flux at the observer,  $F_\nu$ , is given by

$$F_\nu = \begin{cases} (\nu_a/\nu_m)^{1/3} (\nu/\nu_a)^2 F_{\nu, \text{max}}, & \nu_a > \nu, \\ (\nu/\nu_m)^{1/3} F_{\nu, \text{max}}, & \nu_m > \nu > \nu_a, \\ (\nu/\nu_m)^{-(p-1)/2} F_{\nu, \text{max}}, & \nu_c > \nu > \nu_m, \\ (\nu_c/\nu_m)^{-(p-1)/2} (\nu/\nu_c)^{-p/2} F_{\nu, \text{max}}, & \nu > \nu_c. \end{cases} \quad (30)$$

where  $F_{\nu, \text{max}}$  is the observed peak flux at distance  $d_L$  from the source.

For  $\nu_m > \nu_c$ , called the fast cooling case, the spectrum is

$$F_\nu = \begin{cases} (\nu_a/\nu_c)^{1/3} (\nu/\nu_a)^2 F_{\nu, \text{max}}, & \nu_a > \nu, \\ (\nu/\nu_c)^{1/3} F_{\nu, \text{max}}, & \nu_c > \nu > \nu_a, \\ (\nu/\nu_c)^{-1/2} F_{\nu, \text{max}}, & \nu_m > \nu > \nu_c, \\ (\nu_m/\nu_c)^{-1/2} (\nu/\nu_m)^{-p/2} F_{\nu, \text{max}}, & \nu > \nu_m. \end{cases} \quad (31)$$

As the GRB jet sweeps the interstellar medium, the Lorentz factor of the jet is decelerated. When the Lorentz factor drops below  $\theta^{-1}$ , the jet starts to expand sideways and becomes detectable by the off-axis observers. These afterglows are not associated with the prompt GRB emission. Such *orphan* afterglows are a natural prediction of GRB jets. Radio transient sources probe the high energy population of the Universe and can provide further constraints on the intrinsic rate of GRBs. Even if the prompt emission is highly collimated, the Lorentz factor drops  $\gamma_d < \theta^{-1}$  around the time

$$t_\theta \sim 2.14 \left( \frac{E_{\text{iso}}}{5 \times 10^{54}} \right)^{1/3} \left( \frac{\theta}{0.1} \right)^{8/3} n^{-1/3} (1+z) \text{ days}, \quad (32)$$

and the jet starts to expand sideways. Finally the shock velocity becomes non-relativistic around the time

$$t_{\text{NR}} \sim 1.85 \times 10^2 \left( \frac{E_{\text{iso}}}{5 \times 10^{54}} \right)^{1/3} \left( \frac{\theta}{0.1} \right)^{2/3} n^{-1/3} (1+z) \text{ days}, \quad (33)$$

(Ioka & Mészáros 2005). After the time  $t_\theta$ , the temporal dependence of the critical break frequencies should be replaced by  $\nu_c \propto t^0$ ,  $\nu_m \propto t^{-2}$ ,  $\nu_a \propto t^{-1/5}$  and  $F_{\nu, \text{max}} \propto t^{-1}$  (Sari et al. 1999). We also use the same evolution in the non-relativistic phase for simplicity, which underestimates the afterglow flux after  $t_{\text{NR}}$ .

Fig. 7 shows the light curves for a typical GRB from Pop III.2 stars assuming an isotropic kinetic energy  $E_{\text{iso}} \sim 5 \times 10^{54} \text{ erg}$  (in proportion to the progenitor mass) as a lower limit. Pop III.1 afterglows are expected to be brighter. Consistently with previous works, we conclude that it is possible to observe the GRB radio afterglows with ALMA, LOFAR, EVLA, and ultimately by SKA.

### 3.2. Upper limits from radio transient survey

In this section, we derive upper limits on the intrinsic GRB rate (including the off-axis GRB) using  $\sim 1$  year timescale radio variability surveys. There are several radio transient surveys completed so far. Bower et al. (2007) used 22 years of archival data from VLA to put an upper limit of  $\sim 6 \text{ deg}^{-2}$  for 1-year variability transients above  $90 \mu\text{Jy}$ , which is equivalent to  $\lesssim 2.4 \times 10^5$  for all sky. Gal-Yam et al. (2006) used FIRST<sup>12</sup> and NVSS<sup>13</sup> radio catalogues to place an upper limit of  $\sim 70$  radio orphan afterglows above 6 mJy in the 1.4 GHz band over the entire sky. This suggests less than  $\sim 10^3$  sources above 1 mJy on the sky, because the number of sources is expected to be proportional to flux limit  $F_{\text{lim}}^{-3/2}$  (assuming Euclidian space and no source evolution) (Gal-Yam et al. 2006).

From Fig. 7, a typical GRB's radio afterglow with isotropic kinetic energy  $E_{\text{iso}} \sim 5 \times 10^{54} \text{ ergs}$  stays above 1 mJy over  $\sim 10^2 - 10^3$  days. Combining the results shown in Figs. 5 and 6, we expect  $\sim 10 - 10^4$  sources ( $40 - 10^4$  events per year  $\times 10^2 - 10^3$  days) above  $\sim 1$  mJy. As a consequence, the most optimistic case for Pop III.2 should be already ruled out by the current observations of radio transient sources, if their luminosity function follows the one assumed in the present paper. Only more conservative models are then viable. Radio transient surveys are not yet able to set upper limits on the Pop III.1 GRB rate. The above conclusion is model dependent, because the afterglow flux depends on the yet uncertain quantities such as the isotropic energy  $E_{\text{iso}}$  and the ambient density  $n$ . If the circumburst density is higher than usual, the constraints from the radio transient surveys would be even severer.

In Figs. 8-9, we show the predicted observable GRB rate  $dN_{\text{GRB}}^{\text{obs}}/dz$  in Eq. (26) for Pop III.1 and III.2 detectable by *Swift*, SVOM, JANUS and EXIST missions.

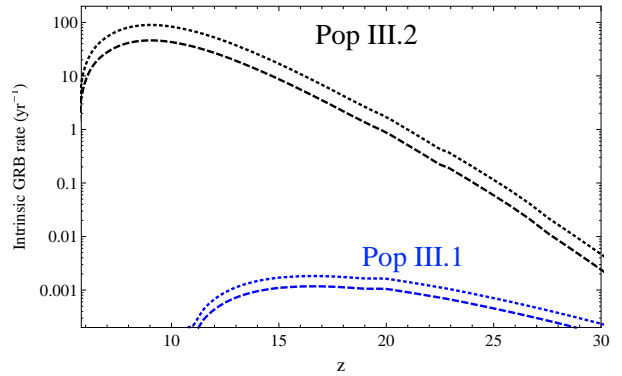


**Fig. 5.** The intrinsic GRB rate  $dN_{\text{GRB}}/dz$ , the number of (on-axis + off-axis) GRBs per year on the sky in Eq. (28), as a function of redshift. We set  $f_* = 0.001$  and  $v_{\text{wind}} = 100 \text{ km/s}$  for this plot. For Pop III.2 with Salpeter IMF (dashed black line) and with Gaussian IMF (dotted black line). For Pop III.1 with Salpeter IMF (dashed blue line) and with Gaussian IMF (dotted blue line).

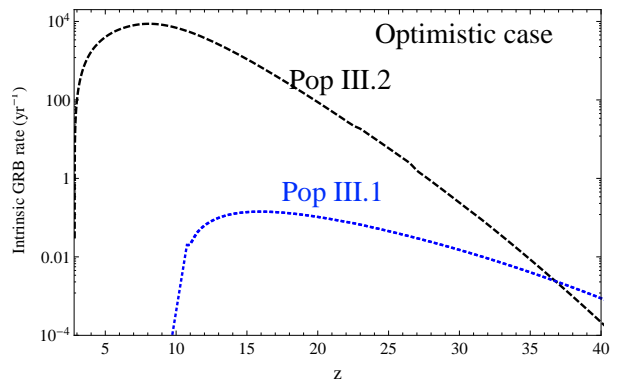


**Fig. 6.** The intrinsic GRB rate  $dN_{\text{GRB}}/dz$ , the number of (on-axis + off-axis) GRBs per year on the sky in Eq. (28), as a function of redshift for our optimistic model assuming a high star formation efficiency,  $f_* = 0.1$ , slow chemical enrichment,  $v_{\text{wind}} = 50 \text{ km/s}$ , and a Gaussian IMF, for both Pop III.2 (dashed black line) and Pop III.1 (dotted blue line).

The shown results are still within the bounds from available upper limits from the radio transient surveys. Overall, it is more likely to observe Pop III.2 GRBs than Pop III.1, but the predicted rate strongly depends on the IGM metallicity evolution and the star formation efficiency. The dependence on the IMF is relatively small.

Fig. 10 shows the GRB rate expected for EXIST observations. We use the rate which is within the constraints by the current observations of radio transients. We expect to observe  $N \sim 6$  GRBs per year at  $z > 6$  for Pop III.2 and  $N \sim 0.01$  per year for Pop III.1 at  $z > 10$  at a maximum.

## 4. Conclusion and Discussion

There are yet no direct observations of Population III stars, despite much recent development in theoretical studies on the formation of the early generation stars.

<sup>12</sup> <http://sundog.stsci.edu/>

<sup>13</sup> <http://www.cv.nrao.edu/nvss/>

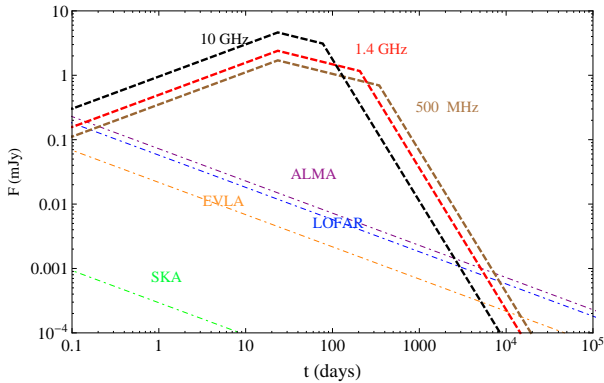


**Fig. 7.** The theoretical light curve of radio afterglow of a typical Pop III.2 GRB at  $z \sim 10$ . We show the evolution of afterglow flux  $F$  (mJy) as a function of time  $t$  (days) for typical parameters: isotropic kinetic energy  $E_{\text{iso}} \sim 5 \times 10^{54}$  erg, electron spectral index  $p = 2.5$ , plasma parameters  $\epsilon_e = 0.1$ ,  $\epsilon_B = 0.01$ , initial Lorentz factor  $\gamma_d = 200$ , interstellar medium density  $n = 1 \text{ cm}^{-3}$ , for the range of frequencies: 500 MHz (dashed brown line), 1.4 GHz (dashed red line), 10 GHz (dashed black line), in comparison with flux sensitivity  $F_{\nu}^{\text{sen}}$  as a function of integration time,  $t_{\text{int}}$  (days) for SKA (dot-dashed green line), EVLA (dot-dashed orange line), LOFAR (dot-dashed blue line) and ALMA (dot-dashed purple line).

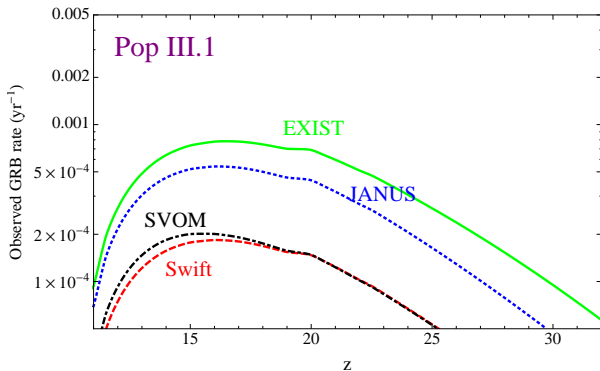


**Fig. 8.** Predicted Pop III.1 GRB rate observed by *Swift*, dashed red line, *SVOM*, dot-dashed black line, *JANUS*, dotted blue line and *EXIST*, green line. We adopt a GRB rate model that is consistent with the current upper limits from the radio transients; Gaussian IMF,  $v_{\text{wind}} = 50 \text{ km/s}$ ,  $f_* = 0.1$ .

In this paper, we follow a recent suggestion that massive Pop III stars could trigger collapsar gamma-ray bursts. Observations of such energetic GRBs at very high redshifts will be a unique probe of the high redshift Universe. Using a semi-analytical approach we estimate the star formation rate for Pop III.1 and III.2 stars including all relevant feedback effects: photo-dissociation, reionization and metal enrichment.

Orphan afterglows are a natural prediction of GRB jets. Using radio transient sources we are able to derive constraints on the intrinsic rate of GRBs. We estimate the

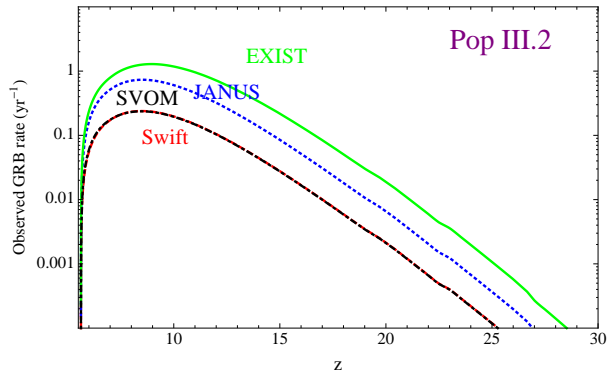


**Fig. 9.** Predicted Pop III.2 GRB rate observed by *Swift*, dashed red line, *SVOM*, dot-dashed black line, *JANUS*, dotted blue line, and *EXIST*, green line, for our model with Salpeter IMF,  $v_{\text{wind}} = 100 \text{ km/s}$ ,  $f_* = 0.005$ .

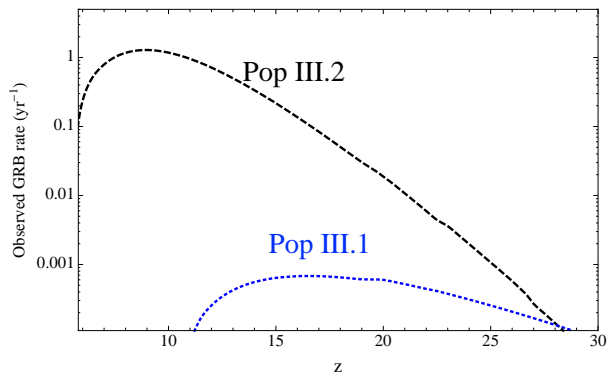


**Fig. 10.** Predicted maximum GRB rate observed by *EXIST*. Pop III.1 GRBs (dotted blue line) and Pop III.2 GRB (dashed black line) for our model with Salpeter IMF,  $v_{\text{wind}} = 100 \text{ km/s}$ ,  $f_* = 0.005$  for Pop III.2 and Gaussian IMF,  $v_{\text{wind}} = 50 \text{ km/s}$ ,  $f_* = 0.1$  for Pop III.1.

predicted GRB rate for both Pop III.1 and Pop III.2 stars, and argue that the latter is more likely to be observed with future experiments. We expect to observe maximum of  $N \lesssim 6$  GRBs per year at  $z > 6$  for Pop III.2 and  $N \lesssim 0.01$  per year for Pop III.1 at  $z > 10$  with *EXIST*.

We also expect a larger number of radio afterglows than X-ray prompt emission because the radio afterglow is long-lived, for  $\sim 1$  yr above  $\sim 1$  mJy from Fig. 7. Combining with the intrinsic GRB rate and constraints from radio transients, we expect roughly  $\sim 10 - 1000$  radio afterglows above  $\gtrsim 1$  mJy already on the sky. They are indeed detectable by ALMA, EVLA, LOFAR and SKA, and even have been already detected by  $\sim 1$  yr timescale variability surveys. We show that using a semi-analytical approach combined with the current surveys such as NVSS and FIRST, we are already able to constrain the Pop III.2 GRB event rate.

Finally, it is important to note that our knowledge on the first stars and GRBs is still limited, and there are uncertainties in their properties, most importantly in their characteristic mass. Recently, Clark et al. (2011)

and Greif et al. (2011) performed cosmological simulations using a sink particle technique to follow the evolution of a primordial protostellar accretion disk. They found that the disk gravitationally fragments to yield multiple protostellar seeds. Although the final mass distribution of the formed stars is still uncertain, formation of multiple systems, especially massive binary Pop III stars, would increase the rate of high-redshift GRBs (e.g., Bromm & Loeb (2006); Fryer & Heger (2005) and references therein). If the GRB fraction per collapse  $f_{\text{GRB}}$  in Eq. (23) is much larger than the current one, say  $f_{\text{GRB}} \sim 1$ , the Pop III.1 GRBs might also become detectable with the radio telescopes ( $\sim 300$  afterglows above  $\sim 1$  mJy on the sky) and the X-ray satellites ( $\sim 1$  event per year for EXIST) in the future.

*Acknowledgements.* R.S.S. thanks the Brazilian agency CNPq (200297/2010-4) for financial support. This work was supported by World Premier International Research Center Initiative (WPI Initiative), MEXT, Japan. We thank Emille Ishida, Andrea Ferrara, Kenichi Nomoto, Jarrett Johnson, and Yudai Suwa for fruitful discussion and suggestions. NY acknowledges the financial support by the Grants-in-Aid for Young Scientists (S) 20674003 by the Japan Society for the Promotion of Science. KI acknowledges the financial support by KAKENHI 21684014, 19047004, 22244019, 22244030.

## References

- Abel, T., Bryan, G. L., & Norman, M. L. 2002, *Science*, 295, 93
- Barkov, M. V. 2010, *Astrophysical Bulletin*, 65, 217
- Belczynski, K., Holz, D. E., Fryer, C. L., et al. 2010, *The Astrophysical Journal*, 708, 117
- Bower, G. C., Saul, D., Bloom, J. S., et al. 2007, *ApJ*, 666, 346
- Bromm, V. & Loeb, A. 2003, *Nature*, 425, 812
- Bromm, V. & Loeb, A. 2006, *ApJ*, 642, 382
- Bromm, V., Yoshida, N., Hernquist, L., & McKee, C. F. 2009, *Nature*, 459, 49
- Chandra, P., Frail, D. A., Fox, D., et al. 2010, *ApJ*, 712, L31
- Ciardi, B. & Loeb, A. 2000, *ApJ*, 540, 687
- Clark, P. C., Glover, S. C. O., Smith, R. J., et al. 2011, *Science*, 331, 1040
- Falcone, A. D., Burrows, D. N., Barthelmy, S., et al. 2009, in *Society of Photo-Optical Instrumentation Engineers (SPIE) Conference Series*, Vol. 7435, Society of Photo-Optical Instrumentation Engineers (SPIE) Conference Series
- Frail, D. A., Cameron, P. B., Kasliwal, M., et al. 2006, *ApJ*, 646, L99
- Frebel, A., Johnson, J. L., & Bromm, V. 2007, *MNRAS*, 380, L40
- Fryer, C. L. & Heger, A. 2005, *ApJ*, 623, 302
- Furlanetto, S. R. & Loeb, A. 2005, *ApJ*, 634, 1
- Gal-Yam, A., Ofek, E. O., Poznanski, D., et al. 2006, *ApJ*, 639, 331
- Gou, L. J., Mészáros, P., Abel, T., & Zhang, B. 2004, *ApJ*, 604, 508
- Greif, T., Springel, V., White, S., et al. 2011, *ArXiv e-prints*
- Greif, T. H. & Bromm, V. 2006, *MNRAS*, 373, 128
- Greiner, J., Krühler, T., Fynbo, J. P. U., et al. 2009, *ApJ*, 693, 1610
- Grindlay, J. E. 2010, in *American Institute of Physics Conference Series*, Vol. 1279, American Institute of Physics Conference Series, ed. N. Kawai & S. Nagataki, 212–219
- Guetta, D., Piran, T., & Waxman, E. 2005, *ApJ*, 619, 412
- Heger, A. & Woosley, S. E. 2002, *ApJ*, 567, 532
- Hernquist, L. & Springel, V. 2003, *MNRAS*, 341, 1253
- Inoue, S., Omukai, K., & Ciardi, B. 2007, *MNRAS*, 380, 1715
- Ioka, K. 2003, *ApJ*, 598, L79
- Ioka, K. & Mészáros, P. 2005, *ApJ*, 619, 684
- Jarosik, N., Bennett, C. L., Dunkley, J., et al. 2011, *ApJS*, 192, 14
- Johnson, J. L. 2010, *MNRAS*, 404, 1425
- Johnson, J. L. & Bromm, V. 2006, *MNRAS*, 366, 247
- Kawai, N., Kosugi, G., Aoki, K., et al. 2006, *Nature*, 440, 184
- Komissarov, S. S. & Barkov, M. V. 2010, *MNRAS*, 402, L25
- Lamb, D. Q. & Reichart, D. E. 2000, *ApJ*, 536, 1
- Langer, N. & Norman, C. A. 2006, *ApJ*, 638, L63
- Lehnert, M. D., Nesvadba, N. P. H., Cuby, J., et al. 2010, *Nature*, 467, 940
- Lewis, A., Challinor, A., & Lasenby, A. 2000, *ApJ*, 538, 473
- Li, L. 2008, *MNRAS*, 388, 1487
- Machacek, M. E., Bryan, G. L., & Abel, T. 2001, *ApJ*, 548, 509
- Mackey, J., Bromm, V., & Hernquist, L. 2003, *ApJ*, 586, 1
- Madau, P., Ferrara, A., & Rees, M. J. 2001, *ApJ*, 555, 92
- Mészáros, P. 2006, *Reports on Progress in Physics*, 69, 2259
- Mészáros, P. & Rees, M. J. 2010, *ApJ*, 715, 967
- Nagakura, H., Suwa, Y., & Ioka, K. 2011, *ArXiv e-prints*
- Nakamura, F. & Umemura, M. 2001, *ApJ*, 548, 19
- Naoz, S. & Bromberg, O. 2007, *MNRAS*, 380, 757
- Omukai, K. & Palla, F. 2003, *ApJ*, 589, 677
- Omukai, K., Tsuribe, T., Schneider, R., & Ferrara, A. 2005, *ApJ*, 626, 627
- O’Shea, B. W. & Norman, M. L. 2008, *ApJ*, 673, 14
- Paul, J., Wei, J., Basa, S., & Zhang, S. 2011, *ArXiv e-prints*
- Pawlik, A. H., Schaye, J., & van Scherpenzeel, E. 2009, *MNRAS*, 394, 1812
- Salvaterra, R., Campana, S., Chincarini, G., Covino, S., & Tagliaferri, G. 2008, *MNRAS*, 385, 189
- Salvaterra, R., Della Valle, M., Campana, S., et al. 2009, *Nature*, 461, 1258
- Sari, R., Piran, T., & Halpern, J. P. 1999, *ApJ*, 519, L17
- Sari, R., Piran, T., & Narayan, R. 1998, *ApJ*, 497, L17

- Scannapieco, E., Schneider, R., & Ferrara, A. 2003, *ApJ*, 589, 35
- Schaerer, D. 2002, *A&A*, 382, 28
- Sheth, R. K. & Tormen, G. 1999, *MNRAS*, 308, 119
- Suwa, Y. & Ioka, K. 2011, *ApJ*, 726, 107
- Tanvir, N. R., Fox, D. B., Levan, A. J., et al. 2009, *Nature*, 461, 1254
- Toma, K., Sakamoto, T., & Meszaros, P. 2010, arXiv:1008.1269v1
- Tornatore, L., Ferrara, A., & Schneider, R. 2007, *MNRAS*, 382, 945
- Totani, T. 1997, *ApJ*, 486, L71+
- Totani, T., Kawai, N., Kosugi, G., et al. 2006, *PASJ*, 58, 485
- Trenti, M. & Stiavelli, M. 2009, *ApJ*, 694, 879
- Wanderman, D. & Piran, T. 2010, *MNRAS*, 406, 1944
- Willott, C. J., McLure, R. J., & Jarvis, M. J. 2003, *ApJ*, 587, L15
- Wise, J. H. & Abel, T. 2005, *ApJ*, 629, 615
- Wyithe, J. S. B. & Loeb, A. 2003, *ApJ*, 586, 693
- Yonetoku, D., Murakami, T., Nakamura, T., et al. 2004, *ApJ*, 609, 935
- Yoshida, N., Abel, T., Hernquist, L., & Sugiyama, N. 2003, *ApJ*, 592, 645
- Yoshida, N., Oh, S. P., Kitayama, T., & Hernquist, L. 2007, *ApJ*, 663, 687
- Yoshida, N., Omukai, K., Hernquist, L., & Abel, T. 2006, *ApJ*, 652, 6